PROCEEDINGS OF SCIENCE

# Precision Measurement of Cosmic Ray Deuterons with Alpha Magnetic Spectrometer

**Carlos Delgado**[a,*] **AMS**

[a] *CIEMAT,*
*Avda. Complutense 40, Madrid, Spain*

*E-mail:* carlos.delgado@ciemat.es

Deuterons are among the most abundant secondary cosmic-ray nucleu. The deuteron flux rigidity dependence provides unique information about the propagation of cosmic rays compared to heavier Li, Be and B fluxes. AMS large acceptance and precise particle rigidity and velocity measurements allow accurate determination of the deuterons flux in the rigidity range from 1.92 to 21.1 GV.

38th International Cosmic Ray Conference (ICRC2023)
26 July - 3 August, 2023
Nagoya, Japan



*Speaker





PoS(ICRC2023)079

## 1. Introduction

Big Bang Nucleosynthesis predicts a very small production of deuterium (D), which is known to be consumed in the nuclear processes occurring during stellar evolution. Consequently, deuterium and its isotopes are not expected to be accelerated in supernova remnants like primary CRs such as protons, helium–4 ($^4$He), carbon (C), and oxygen (O). Instead, they are believed to originate from fragmentation interactions between $^4$He, C, O, and other heavier nuclei with the interstellar medium (ISM); hence, they are classified as secondary CRs [1]. Secondary CRs serve as invaluable probes for characterizing the propagation process of CRs in the Galaxy. Notably, secondary-to-primary CR ratios directly correspond to the amount of material CRs traverse. This measurement is frequently derived from the boron-to-carbon ratio (B/C). The B/C ratio elucidates the diffusive motion of CRs in the Galaxy and plays a crucial role in inferring diffusion parameters. In the standard propagation scenario, all CR species are influenced by the same diffusion parameters obtained from the B/C ratio. The sparse data on other secondary-to-primary ratios, especially for lighter nuclei like D/$^4$He and $^3$He/$^4$He, restricts the evaluation of this "universality in propagation" hypothesis. In this context, the D/$^4$He ratio becomes especially interesting: since the mass-over-charge ratio of both species is identical, solar modulation effects should largely cancel each other in the ratio, potentially offering a time-independent measurement, which on the other hand should be fully consistent the $^3$He/$^4$He ratio given that they have a common parent.

Measuring CR deuterons poses significant challenges due to the necessity of differentiating them from the vastly more prevalent protons. Nevertheless, the AMS detector, as detailed subsequently, is designed to cope with this challenge by ensuring high precision over an extensive energy range in rigidity, velocity and charge determination. Its capability has been underscored through the measurement of He isotopes[**?** ].

In these proceedings, wepresent the D/$^4$He result obtenaide after 11 years of AMS data and update and extend in rigidity the $^3$He/$^4$He result in [**?** ]. This is achieved with a novel analysis methodology that enhances the separation capacity for isotopic analysis of CR with spectrometers.

## 2. Introduction

Big Bang Nucleosynthesis predicts s very small production of deuterium (D) wich is known to be destroyed in the nuclear processes that occur during stellar formation. As such, they are not expected to be accelerated in supernova remnants like primary CRs such as protons, helium–4 ($^4$He), carbon (C), and oxygen (O) do. Instead, they are predicted to originate from fragmentation interactions between $^4$He, C, O, and other heavier nuclei with the interstellar medium (ISM), i.e., they are considered secondary CRs [**?** ]. Secondary CRs are probes to characterize the propagation process of CRs in the Galaxy. In particular, secondary-to-primary CRs ratios are directly related to the amount of material traversed by CRs. This value is typically obtained from the boron-to-carbon ratio (B/C), which demonstrate the diffusive motion of CRs in the Galaxy, and is a key component in constraining the diffusion parameters. Since in the standard propagation scenario all CR species are driven by the same diffusion parameters obtained with the B/C ratio, the lack of information about other secondary-to-primary ratios, especially lighter nuclei like D/$^4$He and $^3$He/$^4$He, has not allowed rigorous testing of this “universality in propagation” postulate. In this regards the D/$^4$He is

specially interesting, since the mass over charge ratio of both species is the same, so it is expected that solar modulation effects will largely cancel in the ratio, potentially providing a time independent measurement.

Measuring CR deuterons is challenging due to the need to separate them from the much more abundant protons, yet the AMS detector, described below, is exquisitely designed to overcome such challenge with high precision in a wide energy range. This has been demonstrated with the measurement of He isotopes[**?** ]. This requires to measure the mass distribution of the particles traversing the detector, rigidity and

In these proceedings we briefly introduce a novel analysis that improves the separation power for isotopic analysis of CR with spectrumeters, and present the D/$^4$He result after 11 years of AMS data, as well as an update to the $^3$He/$^4$He result extended in rigidity.

## 3. AMS Detector

The layout of the detector is shown in Fig. 1. The key elements are the permanent magnet [4], the silicon tracker [5], four planes of time of flight (TOF) scintillation counters [6], the array of anticoncidence counters (ACCs) [7], the transition radiation detector (TRD) [8], the ring imaging Čerenkov detector (RICH) [9], and the electromagnetic calorimeter (ECAL) [10]. The AMS coordinate system is concentric with the magnet. The $x$ axis is parallel to the main component of the magnetic field. The ($y$-$z$) plane is the bending plane. Above, below, and downward- going refer to the AMS coordinate system. The central field of the magnet is 1.4 kG. Before flight, the field was measured in 120 000 locations to an accuracy of better than 2 G. On orbit, the magnet temperature varies from −3 to +20°C. The field strength is corrected with a measured temperature dependence of −0.09%/°C.

The tracker has nine layers, the first ($L1$) at the top of the detector, the second ($L2$) just above the magnet, six ($L3$ to $L8$) within the bore of the magnet, and the last ($L9$) just above the ECAL. $L2$ to $L8$ constitute the inner tracker. Each layer contains double-sided silicon microstrip detectors, which independently measure the $x$ and $y$ coordinates. The tracker accurately determines the trajectory of cosmic rays by multiple measurements of the coordinates with a resolution in each layer of 5–10 $\mu$m in the bending ($y$) direction for different nuclei [11]. Together, the tracker and the magnet measure the rigidity $R$ of charged cosmic rays, with a maximum detectable rigidity of up to 3.5 TV over the 3 m lever arm from $L1$ to $L9$. Each layer of the tracker provides an independent measurement of the charge $Z$ with a resolution of $0.1 < \sigma_Z < 0.8$ for different charge nuclei. Overall, the inner tracker has a resolution of $0.05 < \sigma_Z < 0.3$ for Z=1...28 [12].

As seen from Fig. 1, two of the TOF planes are located above the magnet (upper TOF) and two planes are below the magnet (lower TOF). The overall velocity ($\beta = v/c$) resolution has been measured to be $\sigma(1/\beta) = 0.01 - 0.04$ for different nuclei. This discriminates between upward- and downward-going particles. The pulse heights of the two upper planes are combined to provide an independent measurement of the charge with an accuracy of $\sigma_Z/Z \sim 2\%$. The pulse heights from the two lower planes are combined to provide another independent charge measurement with the same accuracy.

The RICH is located below the two lower TOF planes. Its radiator is located at its top, which is made of two non-overlapping dielectric materials. The radiator consists of 92 tiles of silica aerogel

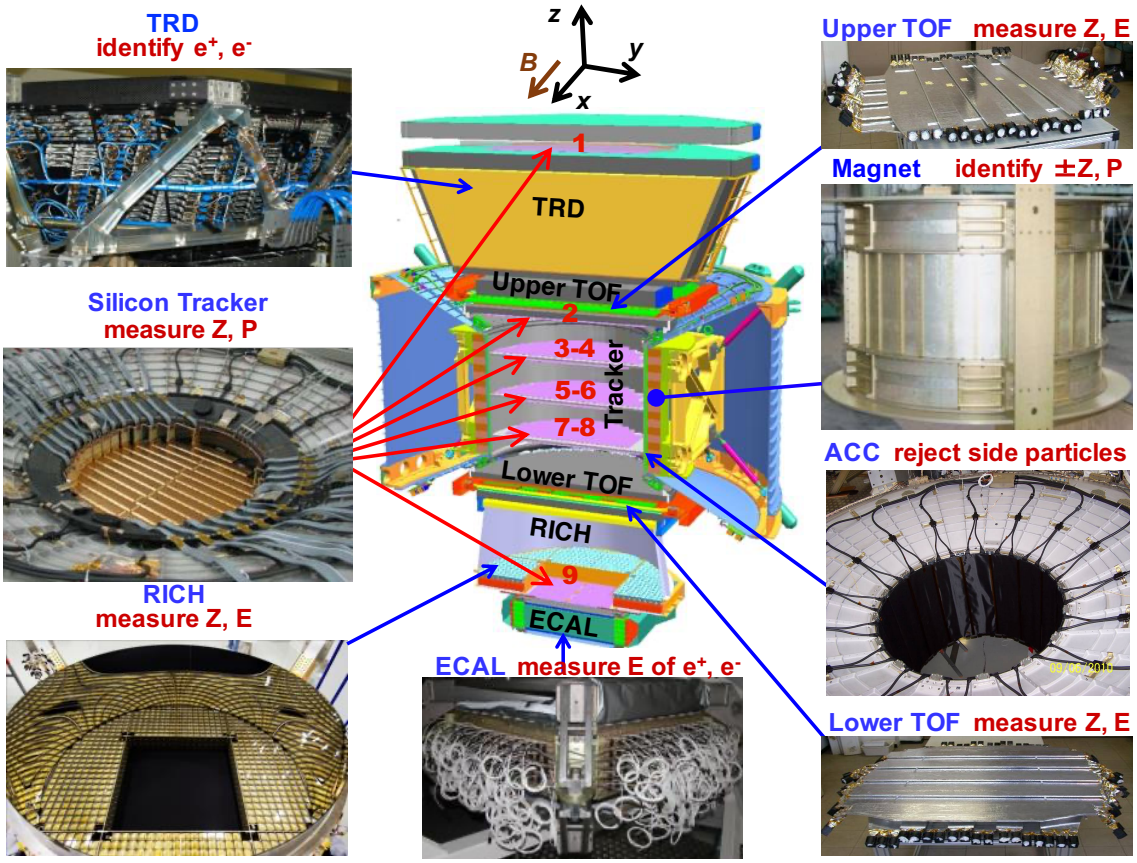


**Figure 1:** The AMS detector showing the main elements and their functions. AMS is a TeV precision, multipurpose particle physics magnetic spectrometer in space. It identifies particles and nuclei by their charge $Z$, energy $E$ and momentum $P$ or rigidity ($R = P/Z$), which are measured independently by the Tracker, TOF, RICH and ECAL. The ACC counters, located in the magnet bore, are used to reject particles entering AMS from the side. The AMS coordinate system is also shown. The $x$ axis is parallel to the main component of the magnetic field and the $z$ axis is pointing vertically.

with dimensions $11.5 \times 11.5 \times 2.5\ cm^3$ and a refraction index of 1.05 and, in the central part, of 16 tiles of sodium fluoride with dimensions $8.5 \times 8.5 \times 0.5\ cm^3$ and a refraction index of 1.33. Its velocity resolution has been measured to be $\sigma(\beta)/\beta = 1.3 \times 10^{-3}$ for charge 1 particles crossing the aerogel radiator, and $\sigma(\beta)/\beta = 3.2 \times 10^{-3}$ for the sodium fluoride one.

Cosmic ray nuclei traversing the AMS were triggered and flagged by the logical OR of any of three trigger conditions: (i) the coincidence, within 240 ns, of signals from all four TOF planes each with a pulse height above 0.5 of a minimum ionizing particle signal (MIP, $Z$ =1) together with an absence of signals from the ACC; OR (ii) the coincidence, within 240 ns, of signals from all four TOF planes each with pulse heights above 3.5 times a MIP signal together with signals from no more than 4 (2011-2016) or 7 (2016-) out of 8 ACC sectors; OR (iii) the coincidence, within 240 ns, of 3 out of the 4 TOF layers each with pulse heights above 0.5 of a MIP signal and with no ACC requirement. Condition (iii) was prescaled to 1%; i.e., only 1 event out of 100 which met these conditions was passed on to the OR. The efficiency of trigger (iii) was estimated directly from

the data to be above 99.9% for all rigidities using events in which 1 of the 4 TOF layers gave no signal. Trigger (iii) is then used to measure the efficiency of triggers (i) and (ii). The overall trigger efficiency has been measured to be >85% over the entire rigidity range for all nuclei.

Monte Carlo (MC) simulated events were produced using a dedicated program developed by the collaboration based on the GEANT4-10.3 package [13]. The program simulates electromagnetic and hadronic interactions [14] of particles and nuclei in the material of AMS and generates detector responses. The digitization of the signals is simulated precisely according to the measured characteristics of the electronics. The simulated events then undergo the same reconstruction as used for the data.

## 4. Isotopes Flux Measurements

The fluxes of different isotopes are obtained by unfolding the measured bi-dimensional histogram of velocity and rigidity for the two RICH radiators, and for the TOF for particles below the RICH threshold. This methodology reduces the systematic errors due to bin-to-bin migration of finite velocity resolution that affects the template mass fit methods[15].

The unfolding effectively fits the following function to the number of measured events

$$\tilde{N}(R_i, \beta_j) = b\ B^{(ij)} + \sum_{\alpha} \sum_{k} (M_\alpha)_k^{(ij)} (A_\alpha)^k (\epsilon_\alpha)^k T^k (\Phi_\alpha)^k \tag{1}$$

where $\tilde{N}(R_i, \beta_j)$ is the expected number of events of rigidity bin $i$ and velocity bin $j$. The $\alpha$ index runs on all the isotopes being fitted, $(\Phi_\alpha)^k$ represents the isotropic flux for the $k$th rigidity bin $(R_k, R_k + \Delta R_k)$ and isotope $\alpha$. $B^{(ij)}$ represents the histogram of background as determined by the data, and $b$ denotes its normalization. $(M_\alpha)^{(ij)}$ is the response function of the detector for triggered particles, $(A_\alpha)^k$ is the effective acceptance obtained by simulations and corrected for minor discrepancies between the data and simulated events, $(\epsilon_\alpha)^k$ is the measured trigger efficiency, and $T^k$ is the collection time. The free parameters of this fit are the fluxes $(\Phi_\alpha)^k$ and the background normalization $b$. This function is employed to unfold the measured number of events for each rigidity bin and each velocity bin measured with the two RICH radiators and the TOF, if the velocity is below the RICH threshold, with shared $\Phi_\alpha$ values.

Extensive studies were conducted to evaluate the systematic errors. These errors encompass uncertainties in background assessment, trigger efficiency, acceptance computation, velocity resolution functions, and the unfolding method.

The principal background source stems from heavier nuclei interacting above tracker $L$ 1 (thin support structures made of carbon fiber and aluminum honeycomb). The background distribution across velocity and rigidity bins was deduced from data by examining the interaction of particles with $Z > 1$ measured at $L$ 1 and with $Z = 1$ in the inner layer. Primarily, the background arises from $^4He$ interactions generating protons, deuterons, and tritons, a distribution well mimicked by the MC. The flux uncertainty due to background remains under 1% within the rigidity measurement range. The systematic error on the flux linked to the trigger efficiency measurement is under 1% for rigidities below 20 GV. The systematic error associated with evaluating the effective acceptance mainly emerges from the uncertainties in the inelastic cross sections of all materials traversed by nuclei in AMS. These systematic errors are under 2.5% for this analysis's entire energy spectrum.

Finally, systematic error due to unfolding was scrutinized by scanning the regularization parameters and the errors of the response function, as detailed in [15]. The associated error was found to be less than 3% for values under ~20 GV.

## 5. Results

The described analysis methodology has been utilized to update the He isotope fluxes from [2], extending both the analyzed period and the energy range for $^3$He. The ratios of the obtained secondary isotopes fluxes and the primary $^4$He versus rigidity are shown in figure 2 and have been fitted to a power law $CR^{\Delta}$ for $R > 5$ GV.

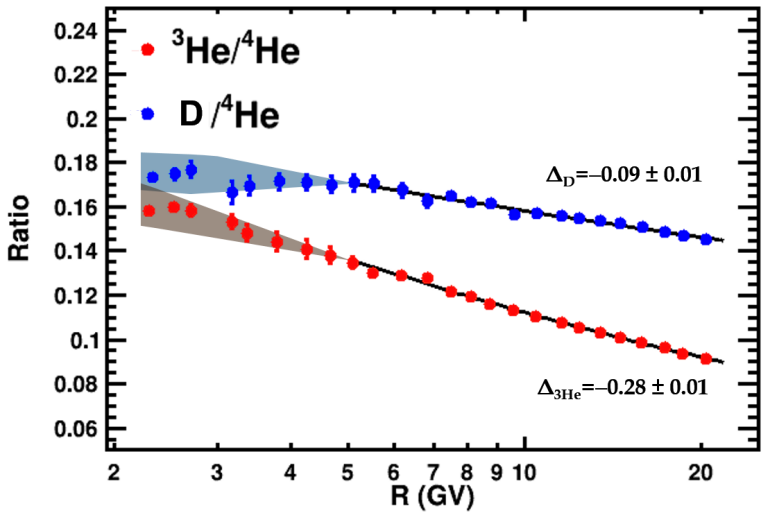


**Figure 2:** Time average measured flux ratios $^3He/^4He$ (red) and $D/^4He$ as a function of rigidity. Only bin-to-bin uncorrelated errors are shown. The shaded areas show the range of time variation of the ratios. The black lines display the results of the fit to the function as explained in the text, and the spectral index for each fit is indicated in the plot.

The comparison of the $D/^4He$ ratio with other measurements and the one from the up-to-date reference models of cosmic rays propagation is depicted in figure 3. Since this ratio is anticipated to be a secondary-to-primary one, the model predicts a shape similar to that of the $B/C$ ratio. Nonetheless, consistent with the discrepancy seen in the $^3He/^4He$ ratio of figure 2, we observe a very significant departure from this expectation.

## 6. Summary and conclusions

The measurement of the deuterium to $^4$He fluxes ratio performed with AMS covers an energy range scarcely explored by previous experiments. Given that this ratio is expected to be nearly independent of solar modulation, as demonstrated in figure 3, it presents an intriguing opportunity to determine cosmic rays propagation parameters. This determination can be made in a manner equivalent to, yet independent of, the $B/C$ ratio.

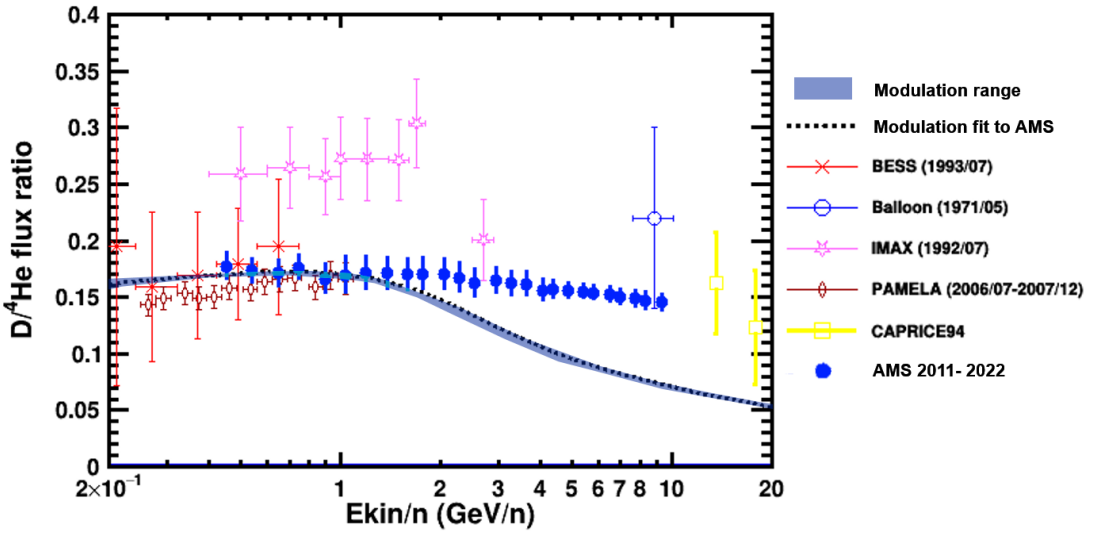


**Figure 3:** AMS measurement of the $D/^4He$ ratio with full errors as a function of the kinetic energy per nucleon (represented by blue filled circles) together with the prediction of the Galprop-Helmod model with parameters from [16] (dashed line). The blue shaded area illustrates the predicted variation range of the ratio due to solar modulation during the AMS measurement period. The other points depict previous measurements of this ratio in literature[17].

However, the measurement exhibits a clear and significant disagreement with one of the reference cosmic rays propagation models previously fitted to AMS data. This discrepancy necessitates an explanation. Both the deuterium to $^4$He and the $^3$He to $^4$He fluxes ratio, as functions of rigidity, are effectively described by a power law. Intriguingly, the spectral index of the deuterium to $^4$He ratio is about three times smaller than that of the $^3$He to $^4$He ratio, with a significance well exceeding $10\sigma$.

This discrepancy suggests that the disagreement between the D and $^3$He ratios with $^4$He and the model cannot be solely attributed to spatial inhomogeneities in propagation parameters. Such inhomogeneities would be expected to affect the measured ratios similarly. Furthermore, the consistent level of the $D/^4He$ ratio across kinetic energy per nucleon or rigidity suggests the need to consider an additional source of D with a spectral shape closer to that of primary cosmic rays.

## References

[1] R. Sina, V. Ptuskin, and ES. Seo, Proceedings of the 28th International Cosmic Ray Conference. Vol. 4, 1973 (2003)

[2] M. Aguilar *et al.*, Physical review letters, Vol. 123, Num. 18, 181102 (2019.

[3] M. Aguilar *et al.*, Physics Reports **894** (2021) 1–116.

[4] K. Lübelsmeyer *et al.*, Nucl. Instrum. Methods Phys. Res., Sect. A **654**, 639 (2011).

[5] B. Alpat *et al.*, Nucl. Instrum. Methods Phys. Res., Sect. A **613**, 207 (2010).

[6] V. Bindi *et al.*, Nucl. Instrum. Methods Phys. Res., Sect. A **743**, 22 (2014).

[7] Ph. von Doetinchem *et al.*, Nucl. Phys. B, Proc. Suppl. 197, 15 (2009).

[8] Th. Kirn, Nucl. Instrum. Methods Phys. Res., Sect. A 706, 43 (2013).

[9] M. Aguilar et al., Nucl. Instrum. Methods Phys. Res., Sect. A 614, 237 (2010); F. Giovacchini Nucl. Instrum. Methods Phys. Res., Sect. A 766, 57 (2014).

[10] C. Adloff *et al.*, Nucl. Instrum. Methods Phys. Res., Sect. A 714, 147 (2013).

[11] G. Ambrosi, V. Choutko, C. Delgado, A. Oliva, Q. Yan, and Y. Li, Nucl. Instrum. Methods Phys. Res., Sect. A **869**, 29 (2017).

[12] Y. Jia, Q. Yan, V. Choutko, H. Liu, and A. Oliva, Nucl. Instrum. Methods Phys. Res., Sect. A **972**, (2020).

[13] J. Allison *et al.*, Nucl. Instrum. Methods Phys. Res., Sect. A **835**, 186 (2016); J. Allison *et al.*, IEEE Trans. Nucl. Sci. **53**, 270 (2006); S. Agostinelli *et al.*, Nucl. Instrum. Methods Phys. Res., Sect. A **506**, 250 (2003).

[14] Q. Yan, V. Choutko, A. Oliva, and M. Paniccia, Nuclear Physics A **996** 121712 (2020).

[15] C. Delgado *et al.*, in preparation.

[16] MJ Boschini *et al.*, The Astrophysical Journal Supplement Series, Vol 250, Num. 2, 27 (2020).

[17] JZ Wang *et al.*, The Astrophysical Journal, Vol. 564, Num. 1, 244 (2002); KMV Apparao, KMV, Proceedings of the 13th International Conference on Cosmic Rays, Vol. 1, OG Sessions, 126 (1973); GA de Nolfo *et al.*, AIP Conference Proceedings, Vol. 528, 425 (2000); O. Adriani et al., The Astrophysical Journal, Vol. 1, 68 (2016); P. Papini et al., The Astrophysical Journal, Vol. 615, 259 (2004).